ACS OMEGA

Open Access

http://pubs.acs.org/journal/acsodf

Review

Review on Lysosomal Metal Ion Detection Using Fluorescent Probes

Akshay Silswal,[†] Kavyashree P.,[†] and Apurba Lal Koner*

Cite This: *ACS Omega* 2024, 9, 13494−13508

Read Online

ACCESS | Metrics & More | Article Recommendations | Supporting Information

ABSTRACT: Metal ions are indispensable and play an important role in living systems. Metal ions coordinated to metalloenzymes pocket activate the bound substrate and labile metal ions maintaining the ionic balance. The amount of metal ions present in various subcellular compartments of the cells is highly regulated for maintaining cellular homeostasis. An imbalance in the metal ion concentration is related to several diseases and results in serious pathological conditions. Mostly the internalized metal ions are processed in the lysosomal compartment of the cell. A delicate regulation of metal ions in the lysosomal compartment can modulate the lysosomal pH and inhibit hydrolytic enzymes, which ultimately causes lysosomal storage disorders. In the past decade, the understanding and regulation of lysosomal metal ions based on fluorometric methods have gained significant attention. In this review, we have comprehensively summarized the development of various fluorescent reporters over the past five years for a selective and sensitive estimation of lysosomal metal ion concentration. We believe this consolidated and timely review will help researchers working in the areas associated with lysosomal metal ions.

1. INTRODUCTION

Metals are essential for all living organisms, serving crucial functions in several fundamental processes such as catalysis, biomineralization, signaling, and osmotic regulation.[1] Out of ten essential metals vital for human physiology, four belong to the main group of elements, including sodium (Na), potassium (K), magnesium (Mg), and calcium (Ca). The remaining six belong to the category of transition metals, including manganese (Mn), iron (Fe), cobalt (Co), copper (Cu), zinc (Zn), and molybdenum (Mo). Mammalian cells have developed intricate metallo-regulatory mechanisms to maintain the balance of these essential metal ions to support various biological processes.[2] However, the reactive oxygen species (ROS) generated in the cellular systems due to abnormal catalytic activity of redox-active metals such as iron and copper cause damage to biomolecules such as proteins, membranes, and nucleic acids. Similarly, the dysregulation in the homeostasis of Fe^{2+}/Fe^{3+}, Cu^{+}/Cu^{2+}, Zn^{2+}, K^{+}, and Ca^{2+} is closely associated with ailments such as atherosclerosis, neurological disorders, epilepsy, and many more. Intracellular upregulation or downregulation of essential metal ions/ion channels is closely linked to different cancers as shown in Figure S1. On the other hand, certain metal ions widely used in industries like Al^{3+}, Hg^{2+}, Cd^{2+}, and Pd^{2+} are toxic to living organisms and interrupt essential biological processes. When inadvertently taken up by cells, these toxic metal ions accumulate within the lysosomal compartment.

Lysosomes are acidic cellular organelles, commonly referred as the "cellular debris", a management center within the eukaryotic cells. They play a crucial role in multiple cellular functions by utilizing hydrolytic enzymes and lysosomal membrane proteins (LMPs). These functions encompass the breakdown of macromolecules, preservation of lysosomal membrane integrity, facilitation of membrane trafficking, and maintenance of ionic gradients. Regulation of multiple metal ion homeostasis occurs through transporter proteins situated in late endosomes and lysosomes.[3] Furthermore, the fusion of lysosomes with endosomes plays a crucial role in the cellular processes of intracellular or extracellular material disposal and recycling, which is termed microautophagy. However, the disrupted degradation of lysosomes is primarily a consequence of oxidative stress, which profoundly impacts cellular functions and contributes to the development of various diseases. Specifically, in the context of oxidative stress, Zn^{2+} ions are responsible for inducing lysosomal membrane permeabilization, a critical process linked to zinc-induced neuronal death in the hippocampus. Positively charged metal ions like Pd^{2+} can interact with either the thiol group of hydrolytic enzymes or negatively charged components leading to inactivation of these enzyme systems. Therefore, monitoring of metal cations at the subcellular compartments like the lysosome level is in demand.

To address this need, fluorescence-based techniques are employed to detect analytes in the cellular environment. These techniques are noninvasive and provide spatiotemporal monitoring with subcellular resolution to observe organelle functions. The presence of metal ions can alter the fluorescence response of probes through mechanisms like photoinduced electron transfer (PET), intramolecular charge transfer (ICT),

Received: October 31, 2023
Revised: February 21, 2024
Accepted: February 27, 2024
Published: March 11, 2024

https://doi.org/10.1021/acsomega.3c08606
ACS Omega 2024, 9, 13494−13508

quenching, chelation-induced enhanced fluorescence (CIEF), and other phenomena.[4,5] Recent research has explored these phenomena to detect various metal ions in the cellular environment and biological samples.[1,6] Specifically, small-molecule fluorescent probes prone to hydrolysis, such as lipophilic amines, are popular for targeting the lysosomal compartment of cells. Given the critical role of lysosomes in maintaining the homeostasis of various metal ions and regulating their signaling, it is essential to monitor metal ion concentrations in lysosomes (Figure 1). Researchers, including us, have

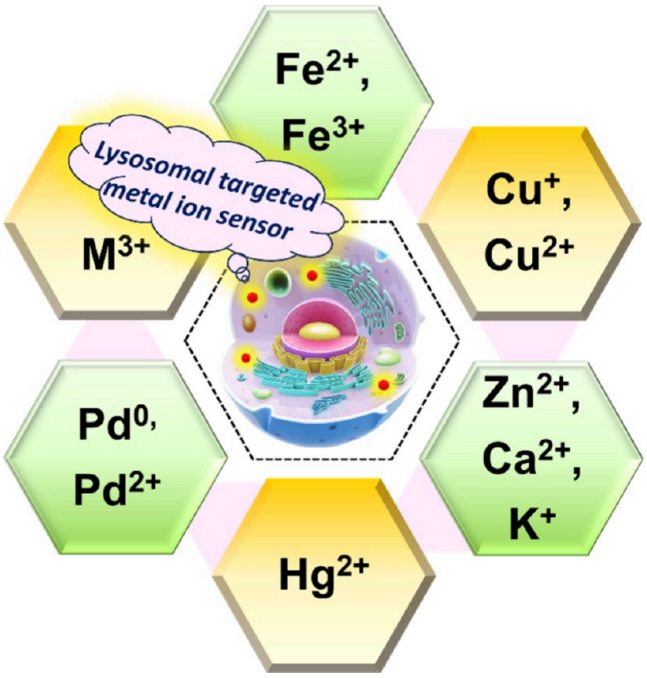

Figure 1. Metal ions associated with lysosomal dysfunctions.

extensively investigated the detection of numerous metal ions within lysosomes and continuously worked on developing the field. This review summarizes recent progress over the past five years and offers insights into future improvements in this field.

2. LYSOSOMAL METAL ION DETECTION

2.1. Detection of Iron (Fe(II) and Fe(III)). Iron plays a pivotal role within cells, participating in essential cellular processes such as DNA synthesis and mitochondrial metabolism. However, it also significantly mediates ferroptosis, a controlled form of cell death triggered by lipid-derived reactive oxygen species (ROS). When iron levels become excessive, they can be potentially toxic due to their unregulated redox activity, particularly labile Fe(II), which refers to loosely protein-bound or free Fe(II) ions, leading to oxidative damage through the Fenton reaction. Lysosomes assume a central function in preserving iron homeostasis while acting as key integrators of metabolic and cell death signals stemming from various subcellular compartments. In a recent review, the intricate role of lysosomes in iron homeostasis was thoroughly explored.[7] In this section, we discuss the development of iron sensors for monitoring metal levels within lysosomes, primarily employing fluorescence techniques.

Hirayama and co-workers reported the Gol-SiRhoNox probe (**1**) as a means to identify labile Fe(II) specifically within the Golgi apparatus.[8] They achieved selective localization without causing the probe to relocate to the inner leaflet of the plasma membrane by incorporating a myristoyl substitution into the probe. Subsequently, they modified the probe through N-oxidation to create the derivative LysoRhoNox (**2**), which is designed to target the lysosome for the detection of labile Fe(II). In HEPES buffer with a pH of 7.4 and containing 30% dioxane, the open form of the silicon-based rhodamine derivative **2** has an absorption peak at 550 nm and emits light at 575 nm. In live SH-SY5Y neuroblastoma cells, the study revealed that VPS35, a crucial regulator of protein transport from endosomes to the trans-Golgi network, is essential for preventing lysosomal accumulation of labile Fe(II). Knockdown of VPS35 led to lysosomal Fe(II) accumulation, which was restored to normal levels by treatment with R55 (molecular chaperone compound) through VPS35 expression recovery. This dysfunction of VPS35 disrupts iron trafficking within the Golgi network and promotes lysosomal Fe(II) accumulation (Figure 2).

Carbon dots find versatile applications in sensing, and the hydrothermal synthesis method has garnered significant scientific interest due to its simplicity and convenience. In 2021, Yang and co-workers introduced yellow emissive carbon dots (CDs, **3**) to detect Fe(III).[9] These CDs were synthesized through the hydrothermal carbonization of dried field mint. They exhibited an average diameter of 6.66 ± 0.83 nm and could tolerate a wide pH range from 3 to 9. The optimal excitation wavelength at 471 nm corresponded to a maximum emission wavelength of 531 nm. The CDs proved effective as a "turn-off" sensor for tracking Fe(III). This is attributed to the presence of carbohydrates, amino acids, alcohols, and flavonoids in the CD composition, which likely resulted in alcohol-, carbonyl-, and nitrogen-containing functional groups on the CD surface. These groups quickly reacted with Fe(III), leading to nonradiative electron transfer, including the partial transfer of an electron in the excited state to the d orbital of Fe(III). This interaction resulted in a noticeable quenching of the CD fluorescence. The CDs exhibited both colorimetric and fluorometric responses to Fe(III), with a low detection limit of 0.037 μM. In addition to their sensing capabilities, the CDs displayed biocompatibility at a concentration of 0.8 mg/mL and were able to localize in lysosomes. This localization allowed for a rapid response to Fe(III) within 40 s, resulting in a decrease in intracellular fluorescence (Figure 3a,b). The authors further explored the practicality of this developed probe for imaging applications in bacteria and zebrafish larvae.

In the same year, Li and colleagues reported using the similar hydrothermal method to synthesize blue-emissive iron and nitrogen co-doped carbon quantum dots (Fe,N-CDs, **4**).[10] Here, ethylenediamine and trisodium citrate were used as the nitrogen and carbon sources, respectively, and $FeCl_3$ was used as the iron source. The maximum emission was observed at 450 nm upon exciting at 365 nm. The prepared Fe,N-CDs showed high selectivity and sensitivity for Fe(III) with a limit of detection (LOD) of 0.64 μM. The cause of fluorescence decrease after the addition of Fe(III) was attributed to the static quenching (Figure 3c–e). Fe,N-CDs were applied to the HeLa cells to detect Fe(III) in the lysosomes.

In 2022, Guo and co-workers designed and synthesized a pH-tolerant rhodamine-based Fe(III) sensor (**5**) with an Fe(III) binding moiety (Figure 4).[11] Upon introduction of Fe(III), compound **5** exhibited increase in absorption at 555 nm, accompanied by a turn-on fluorescence response with emission maximum at 580 nm in acetonitrile/Tris-HCl buffer (10 mM, pH 7.3, v/v 3:1). The probe was selective to Fe(III) in the

https://doi.org/10.1021/acsomega.3c08606
ACS Omega 2024, 9, 13494−13508

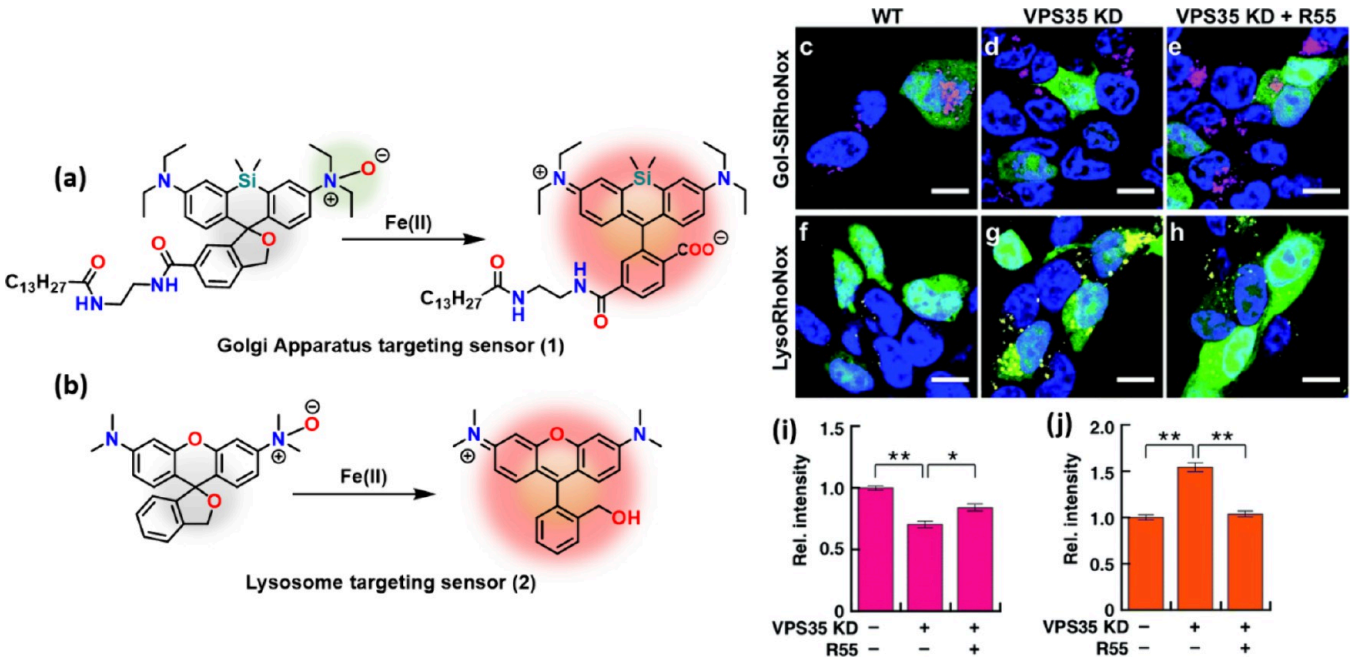

Figure 2. Schematic representation of (a) Golgi apparatus (**1**) and (b) lysosome targeting (**2**) iron sensors and fluorescence microscopy images (c–h) representing the impact of VPS35 knockdown and R55 supplementation on Golgi apparatus (magenta) and lysosomal (yellow) local labile Fe(II) levels in SH-SY5Y cells. The GFP marker (green) was used to assess the efficiency of siRNA transfection specifically in the context of VPS35 knockdown and nuclear staining achieved using Hoechst 33342. Scale bar: 10 μm. Quantitation of fluorescence intensities of originating from the Golgi apparatus (i) and lysosome (j) in GFP positive cells.

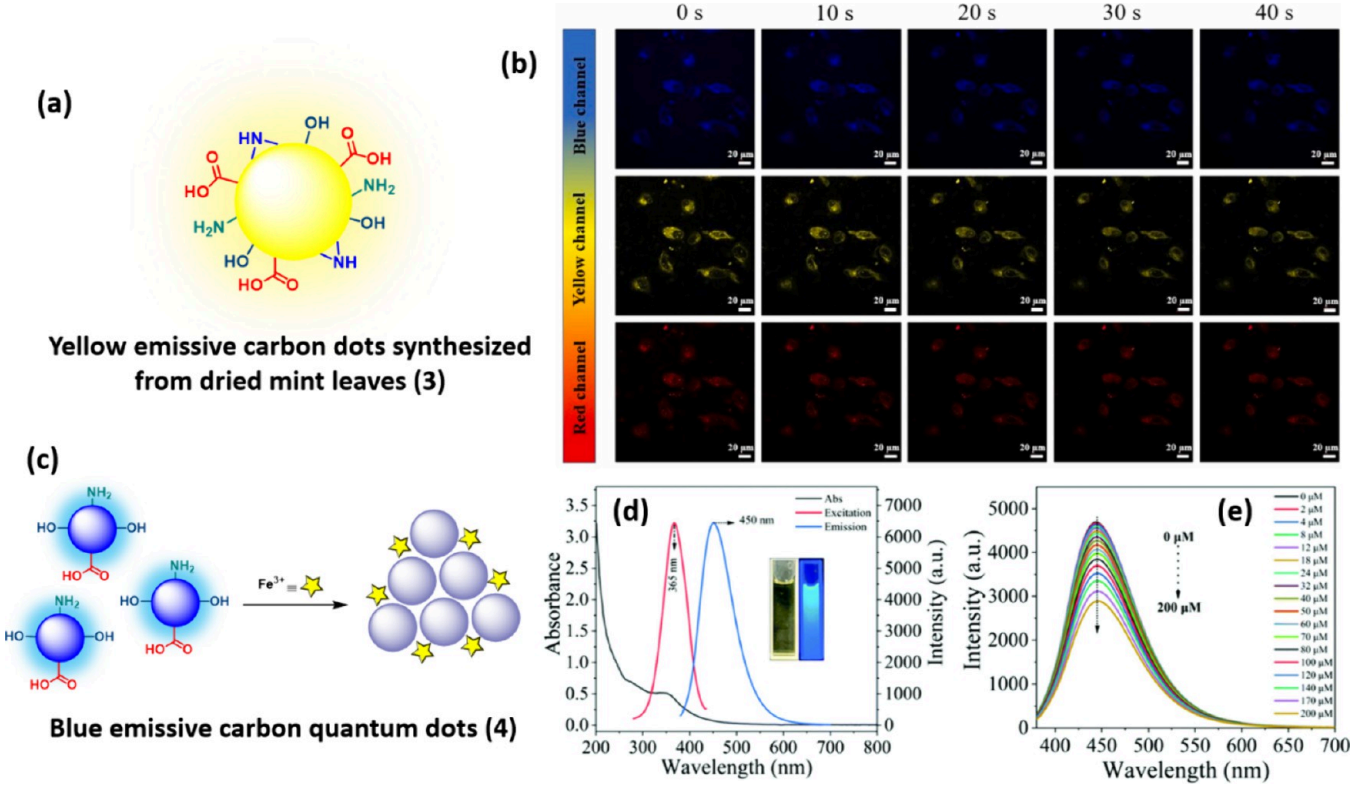

Figure 3. (a) Representation of heteroatoms decorating the surface of carbon dots (**3**). (b) Fluorescence microscopic images depicting the application of carbon dots (**3**) for rapid detection of Fe(III) in lysosomal lumen of live cells Scale bar: 20 μm. (c) Schematic representation of fluorescence emission quenching of carbon quantum dots (**4**) on addition of Fe(III). (b) is reprinted with permission from ref 9. Copyright 2021, Elesvier. (d) Absorption, emission, and excitation spectra of the carbon quantum dots (**4**) and (e) fluorescence response of carbon dots (**4**) with the addition of Fe(III). (d, e) is reprinted with permission from ref 10. Copyright 2021, Royal Society of Chemistry.

https://doi.org/10.1021/acsomega.3c08606
ACS Omega 2024, 9, 13494−13508

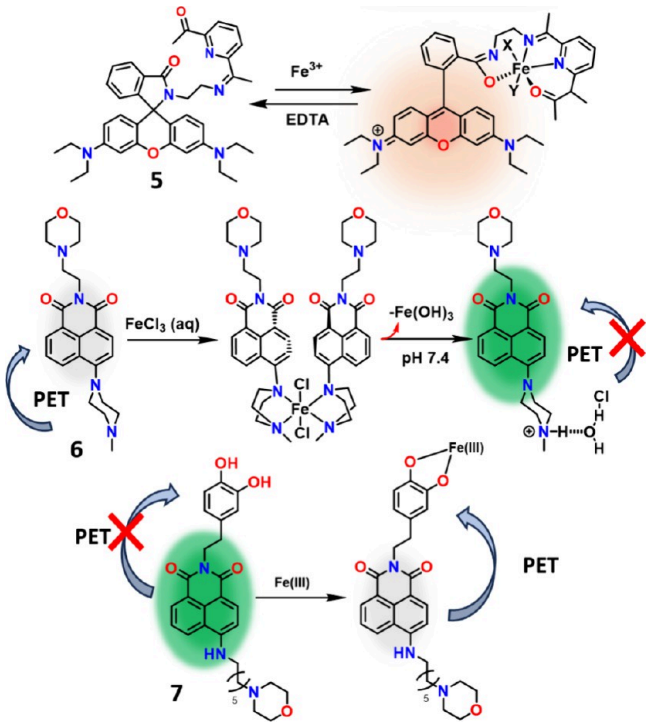

Figure 4. Schematic representation of the mechanism of action in molecules **5**−**7** for sensing Fe(III) ions.

presence of other metal ions as well. The authors elucidated the binding of **5** with Fe(III) in a 1:1 fashion with a binding constant of 1.54×10^7 M^{-1}. The limit of detection for Fe(III) was determined to be 0.05 μM. Furthermore, the researchers explored the application of this probe for detecting labile Fe(III) within the lysosomal compartment of human SH-SY5Y neuroblastoma cells.

Qin and co-workers introduced a 1,8-naphthalimide-based probe (**6**), which incorporates piperazine and morpholine elements for the specific detection of Fe(III) within lysosomes.[12] The probe **6** relies on photoinduced electron transfer from piperazine to the electron-deficient naphthalimide moiety, resulting in the quenching of its fluorescence signal (Figure 4). However, this process ceases in the presence of Fe(III) or HCl, leading to a turn-on fluorescence response. The absorption and emission maxima were identified at 405 and 510 nm, respectively, upon binding to Fe(III) in 2:1 ratio. Probe **6** exhibited a notable increase in fluorescence at 510 nm in the presence of Fe(III) when tested in a 10 mM HEPES buffer (pH 7.4) with an EtOH:H_2O ratio of 5% (v/v). The authors demonstrated the limit of detection of **6** for Fe(III) at 65.2 nM. Furthermore, the authors applied this probe for *in vitro* applications. The probe **6** was able to localize within the lysosomal compartment of cells and effectively sense Fe(III) in HeLa cells.

Our group also demonstrated PET-based 1,8-naphthalimide probe (**7**) for sensing Fe(III) in the lysosomal lumen.[13] We have attached the catechol as a binding moiety for Fe(III) and morpholine for targeting lysosomes. The compound **7** exhibited absorption maxima at 452 nm and emission maxima at 560 nm in MES buffer pH 6.8 (Figure 4). The lysosomal pH does not affect the fluorescence properties of the probe. The binding of catechol to Fe(III) makes it electron deficient, enabling the PET process that decreases the fluorescence intensity. Probe **7** showed 1:1 binding with Fe(III) with a binding constant of (6.9 ± 0.7) $\times 10^4$ M^{-1}. The limit of detection (LOD) was calculated to be 0.44 μM. Further, the probe was applied for the detection and quantitation of lysosomal Fe(III) in live HeLa cells using iron-sorbitex injection.

2.2. Detection of Copper. Copper is the third most abundant metal ion in humans and takes part in several physiological processes owing to its redox activity. It plays a dual role as a structural component and a catalytic cofactor for various enzymes such as copper−zinc superoxide dismutase and cytochrome c oxidase. Within biological environments, copper exists in two distinct oxidation states, Cu^{2+} and Cu^{+}. Typically, the labile intracellular copper ions are predominantly found in the +1 oxidation state. The reduced concentration of Cu^{2+} in humans leads to conditions such as anemia, brain-dysfunction-related diseases, and bone abnormalities.[14] Conversely, an excessive Cu^{2+} concentration can result in kidney and liver damage, and in severe cases, it may lead to death. Notably, the main source of aquatic environmental contamination comes from the waste materials released from chemical industries. As a result, there is an urgent need to monitor Cu^{2+} levels in biotic ecosystems to safeguard human health. This can be accomplished by rationally designing small-molecule-based fluorescent probes.

A series of multifunctional fluorescence compounds **8a**−**d** based on 1,8-naphthalimide were elegantly designed by Qian and their research team (Figure 5a).[15] These compounds served as versatile platforms for comprehensively exploring both Cu^{2+} detection and gene delivery. In aqueous solutions, these probes exhibited distinctive "turn-off" responses when interacting with Cu^{2+} ions (Figure 5b). To be specific, the emission intensity of compounds **8a**−**d** was significantly quenched with reduction factors of 116-, 20-, 12-, and 14-fold, respectively, upon binding with Cu^{2+} ions. Due to their remarkable selectivity and solubility in water, these probes were successfully utilized for real-time imaging of Cu^{2+} in human cervical cancer cells. Moreover, their sensitivity to pH within the range of 4.5−5.5 allowed the specific staining of lysosomal compartments within the cells through the application of complexes **8a**-Cu^{2+} and **8b**-Cu^{2+}.

In 2019, Ye and co-workers demonstrated the selective sensing of Cu^{2+} in CH_3CN-HEPES (4:1, v/v, pH = 7.4) solution using the fluorescent probe 2-butyl-6-(2-ethylidenehydrazinyl)-1*H*-benzo[de]isoquinoline-1,3(2*H*)-dione (**9**) (Figure 5c).[14] The newly reported probe operates using a unique hydrolysis mechanism facilitated by the presence of Cu^{2+}, resulting in the simultaneous quenching of fluorescence. The probe showed excellent selectivity among other metal cations, and the LOD was determined as 320 nM (Figure 5d). Additionally, the viability of the probe for real-time applications was proved by accurately determining the trace amount of Cu^{2+} present in water samples. Furthermore, the authors effectively showcased their ability to detect Cu^{2+} concentrations within the lysosomes of 293T cells (Figure 5e).

Continuing, the Zhu research team of successfully synthesized another fluorescent derivative of naphthalimide known as CuNI (**10**), as shown in Figure 5f.[16] The newly synthesized compound was designed to selectively detect Cu^{2+} ions in an aqueous solution under specific conditions (HOAc-NaOAc buffer, 10 Mm, pH = 5.0). The elegantly designed probe consisted of three components: (i) a morpholine moiety was incorporated to target lysosome within the cellular environment, (ii) 1,8-naphthalimide was utilized as the chromophoric unit to serve as the fluorescent signal, and (iii) 2-picolinyl hydrazide was employed as the responsive group capable of detecting Cu^{2+}

https://doi.org/10.1021/acsomega.3c08606
ACS Omega 2024, 9, 13494−13508

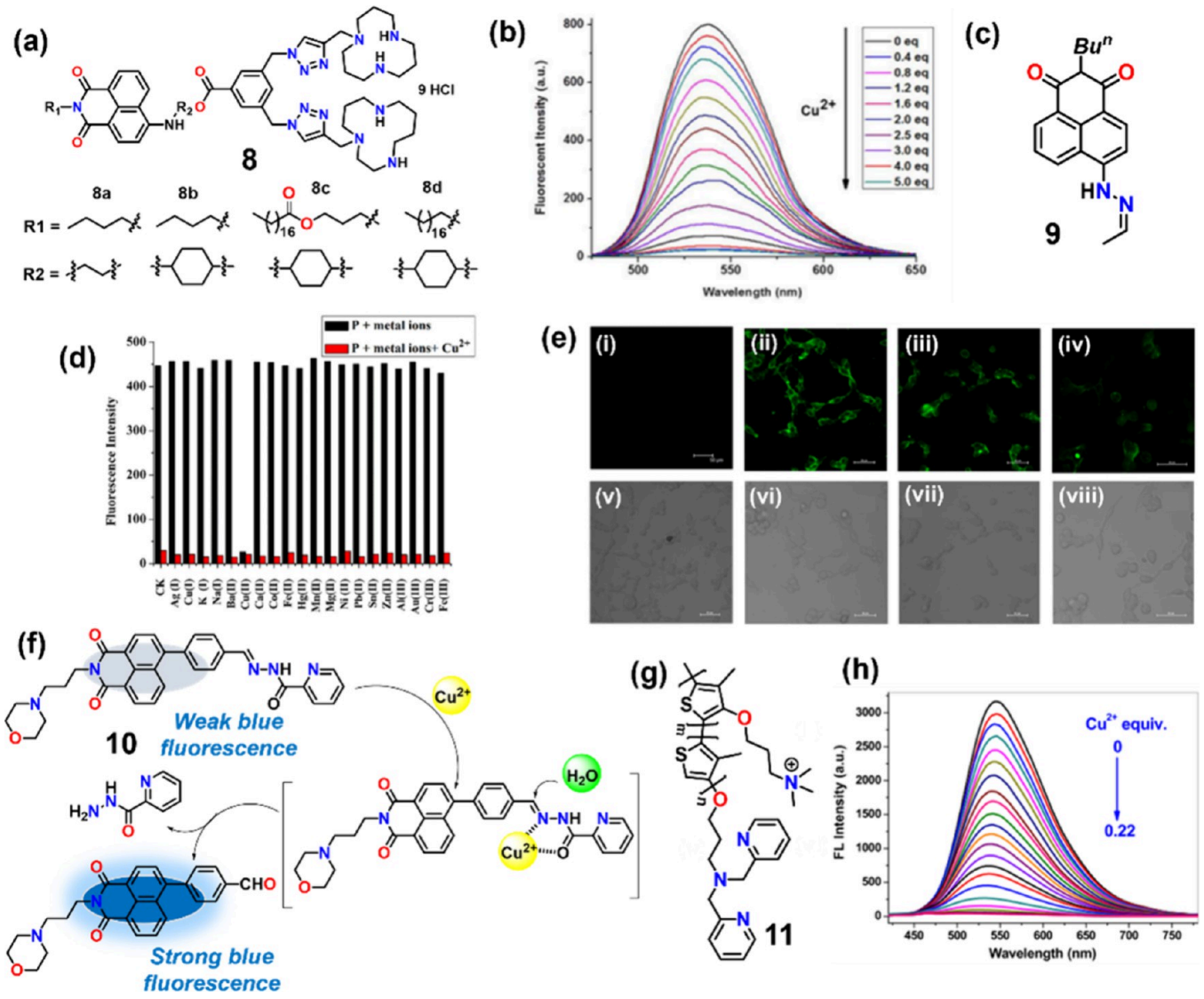

Figure 5. (a, c, g) Chemical structure of chemosensors **8**, **9**, and **11**, respectively. (b) Turn-off response of compound **8** upon gradual addition of Cu^{2+} (0−5.0 equiv). (d) Selectivity assay for probe **9** with various interfering metal cations. (e) Fluorescence images of (i) 293 cells, (ii) probe **9** (10 μM), (iii) probe **9** (10 μM) + Cu^{2+} (10 μM), (iv) probe **9** (10 μM) + Cu^{2+} (20 μM), and (v−viii) the corresponding bright field images, (d, e) is reprinted with permission from ref 14. Copyright 2019, Elesvier. (f) Chemical structure of probe **10** and proposed mechanism for Cu^{2+} detection. (h) Emission spectra of probe **11** (100 μM) in the presence of Cu^{2+} ions (0−22 equiv).

ions. The "turn-on" detection mechanism relied on the hydrolysis of **10**, triggered by the presence of Cu^{2+} ions under acidic conditions. This hydrolysis process led to the formation of the emissive product MFNI; the significant enhancement in the fluorescence intensity was attributed to the aggregation-induced emission (AIE) property of MFNI. Furthermore, the authors investigated the practical applications of this probe in the field of bioimaging. They employed confocal fluorescence microscopy to examine its performance in monitoring lysosomal Cu^{2+} levels in living HepG2 cells, demonstrating its potential as a valuable tool for biological research and diagnostics.

The conjugated polymer PTNPy (**11**) was designed and synthesized by Lu and co-workers for rapid and progressive detection of Cu^{2+} and homocysteine (Hcy) in an aqueous solution (Figure 5g).[17] PTNPy consists of three essential components, namely a polythiophene backbone serving as a fluorophore, dimethylpyridylamine (DPA) acting as a coordinating site for Cu^{2+} ions, and quaternary ammonium salt groups enhancing the water solubility. The chelation of Cu^{2+} with PTNPy resulted in the quenching of PTNPy's fluorescence (Figure 5h). However, the restoration of the emission intensity occurred with the addition of homocysteine to the PTNPy-Cu^{2+} complexes. This phenomenon was ascribed to the release of the free fluorophore due to the stronger coordination interaction between Hcy and Cu^{2+}. The limit of detection for Cu^{2+} was found to be 6.79 nM. The biocompatible probe demonstrated the lysosomal localization and selective sensing of Cu^{2+} ions and HCy in cancer cells (HeLa).

2.2.1. Copper (Cu^{+}). Most of the synthetic fluorescent probes exhibit intensity-based changes upon binding to particular metal ions. However, the main disadvantage of intensity-based probes is their emission response depends on the concentration of the probe uptake into the particular organelle of the cell. Thus, the fluorescence lifetime imaging microscopy (FLIM) technique is a necessary alternative to overcome the limitations of intensity-based probes. These fluorophores demonstrate changes in their

https://doi.org/10.1021/acsomega.3c08606
ACS Omega 2024, 9, 13494−13508

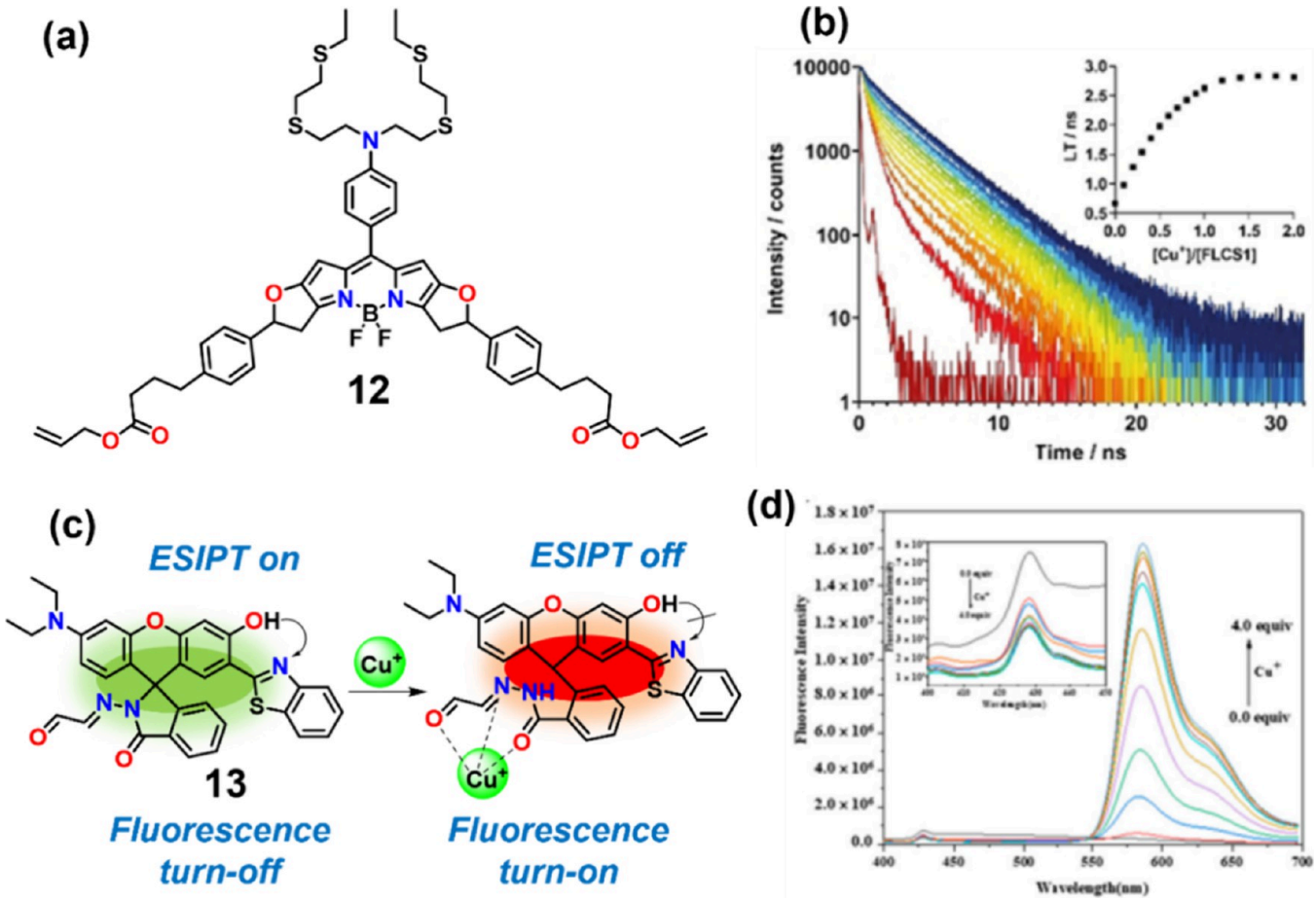

Figure 6. (a) Chemical structure of probe **12**. (b) Fluorescence lifetime decay of probe **12** monitored at 660 nm. Inset: calculated intensity-weighted average lifetime vs Cu^{+}/**12** ratio. (c) Chemical structure and plausible mechanism for recognition of Cu^{+} using **13**. (d) Fluorescence spectra of probe **13** with gradual addition of Cu^{+} (0.0−4.0 equiv).

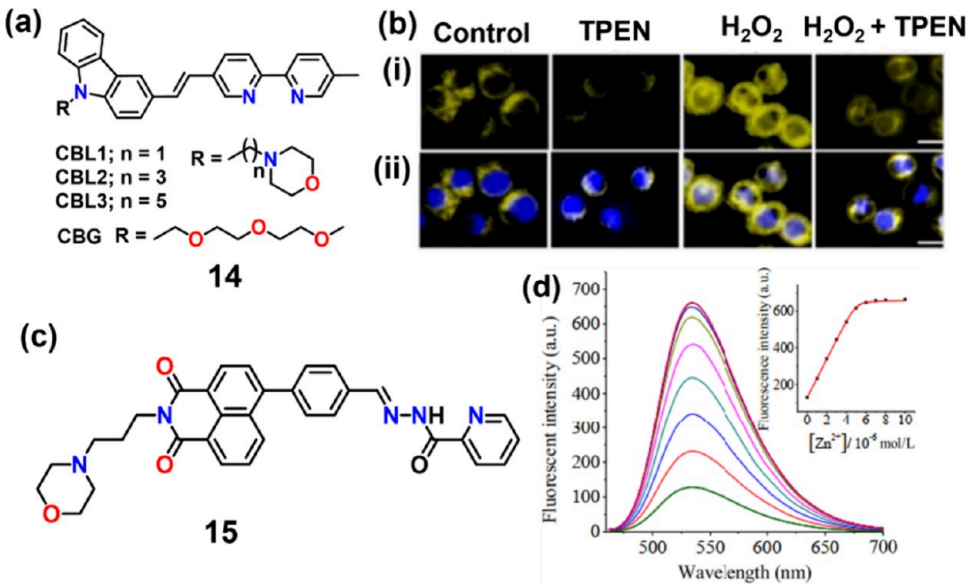

Figure 7. (a) Chemical structure of probe **14**. (b) Fluorescence microscopic images of HeLa cells initially treated with TPEN, H_2O_2, and TPEN + H_2O_2 followed by incubation with CBL2 for 30 min (i) and counter-stained with Hoechst 33342 (ii). Reprinted with permission from ref 20. Copyright 2018, Wiley VCH. (c) Chemical structure of probe **15**. (d) Fluorescence response of probe **15** with increasing concentration of Zn^{2+} in Tris-HCl buffer (0.5% DMSO, pH 5.0). Reprinted with permission from ref 21. Copyright 2019, Elsevier.

fluorescence lifetime upon interacting with the analyte of interest.

In this direction, a BODIPY-based probe FLCS1 (**12**) was reported by Vilar and co-workers, which showed excellent

https://doi.org/10.1021/acsomega.3c08606
ACS Omega 2024, 9, 13494−13508

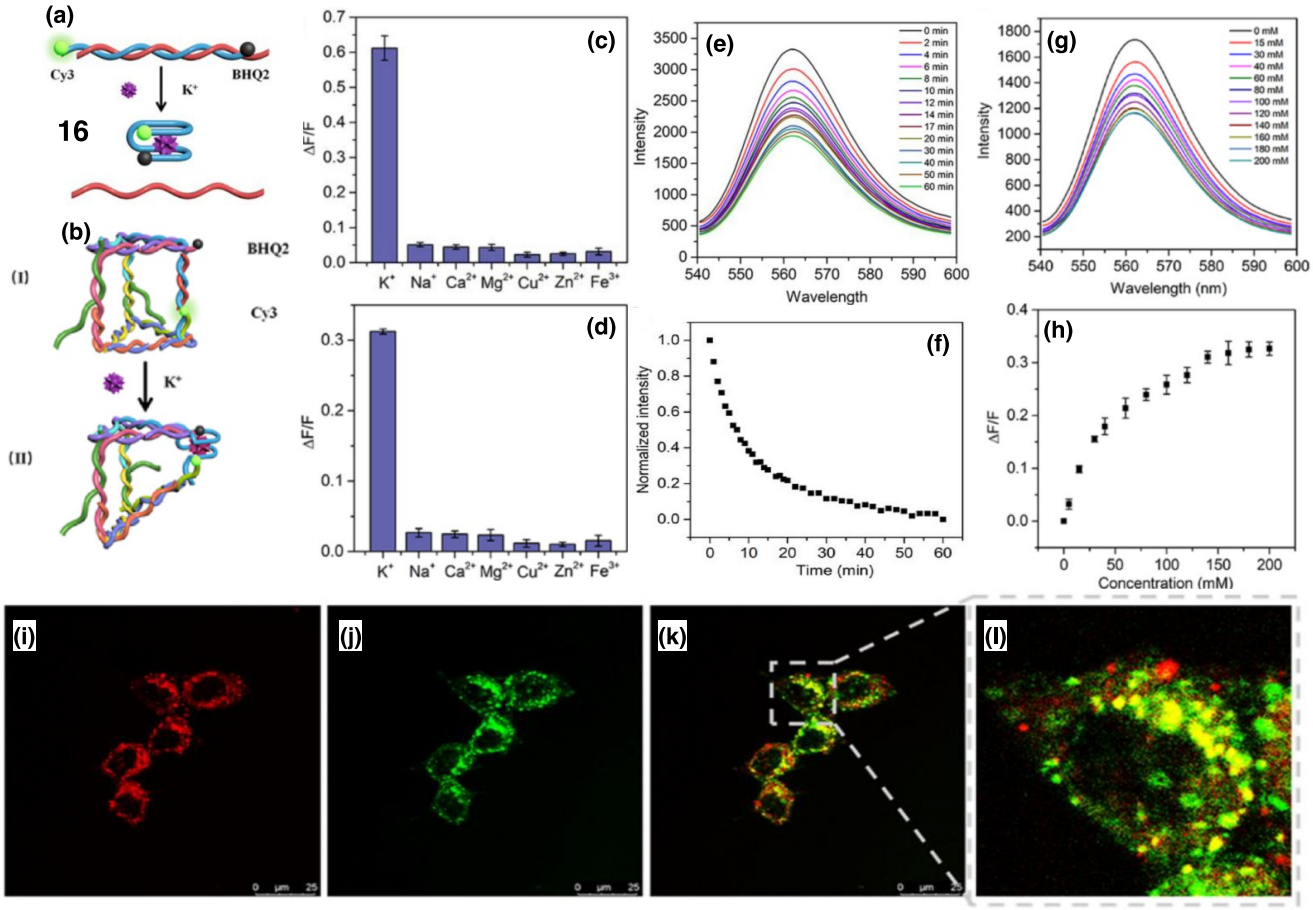

Figure 8. Detection of potassium ions in the lysosomal compartment. (a) Schematic illustration of the conformational changes of K-selective aptamer (KKB). (b) Schematic illustration of the conformational change of **16** with potassium ion. Fluorescence emission intensity ratio ($\Delta F/F$) of 50 nM (c) **16** and (d) KKB with K^+ (150 mM), Na^+ (150 mM), Ca^{2+} (2.0 mM), Mg^{2+} (2.0 mM), Cu^{2+} (50 μM), Zn^{2+} (2.0 mM), and Fe^{3+} (50 μM). (e) Time-dependent emission spectra of **16** with 200 mM potassium ions. (f) Plot of intensity at 562 nm versus time from a time-course experiment. (g) Emission spectra of 50 nM **16** nanoprobes in the presence of increasing concentrations of K^+ (0, 15, 30, 40, 60, 80, 100, 120, 140, 160, 180, and 200 mM). (h) Relationship between the fluorescence emission ratio ($\Delta F/F$) and different concentrations of K^+. (i–l) Colocalization analysis of DTP-Cy5 and Lyso-Tracker dye in MCF7 cells. Yellow fluorescence indicates lysosome-specific localization of the DTP nanoprobe for lysosomal K^+ detection. Reprinted with permission from ref 22. Copyright 2021, American Chemical Society.

selectivity in detecting *in vitro* Cu^+ ions (Figure 6a).[18] The coordination of FLCSI with Cu^+ rendered a remarkable increase in the fluorescence lifetime along with an increment in the fluorescence response (Figure 6b). Incubation of the probe with SH-SY5Y cells revealed the nonlethal response and lysosomal compartmentalization of the probe. In addition, the detection of Cu^+ under live cell conditions was confirmed by the FLIM imaging of the cells treated with the copper-releasing agent CuGTSM.

The He research team introduced an ESIPT-based fluorescent probe known as RBg (**13**) for the detection of aqueous Cu^+ (Figure 6c).[19] This probe initially displayed an emission maximum at 380 nm. However, upon coordination with Cu^+ ions, the emission maximum of the probe shifted to 586 nm with turn-on response (Figure 6d). The limit of detection was determined to be $[Cu^+] = 0.062\ \mu mol\ L^{-1}$. Besides, the binding of Cu^+ ions with RBg led to prominent optical signals within RBg-doped PVDF nanofibers and test strips, illustrating the immediate labeling and recognition of dynamic Cu^+. Moreover, the RBg-Cu^+ complex localized in the lysosomes of the HeLa cells as revealed by the colocalization studies with Lyso-Tracker Green.

2.3. Detection of Zinc (Zn^{2+}). Following iron, the transition metal ion Zn^{2+} is the second most abundant metal ion in the human body. It plays a vital role in regulating immune function, signal transduction, and the operation of metalloenzymes.[20] In healthy individuals, the concentration of Zn^{2+} in serum typically falls within the range of 1−10 μM. In mammalian cells, the Zn^{2+} ions form stable complexes with numerous enzymes, metabolites, and proteins, collectively constituting a labile Zn^{2+} concentration in the picomolar range. The human body accumulates increased levels of Zn^{2+} from the external surroundings. Consequently, disruptions in the concentrations of Zn^{2+} ions can give rise to various health issues, including neurological disorders, cancer, epilepsy, etc.[21] Given its profound implications for human health, there is a compelling need for the accurate and highly sensitive identification of Zn^{2+}.

Recently, Ajayaghosh and co-workers reported the synthesis of a series of self-assembled fluorescent nanoprobes based on carbazole-bipyridine derivatives CBL1−3 and CBG (**14**), as shown in Figure 7a.[20] The authors found that compared to the monomers of CBL1 and CBL3, the CBL2 nanoprobes exhibit promising results in the simultaneous detection of Zn^{2+} and pH variations in lysosomes. The efficiency of the probe to monitor

https://doi.org/10.1021/acsomega.3c08606
ACS Omega 2024, 9, 13494−13508

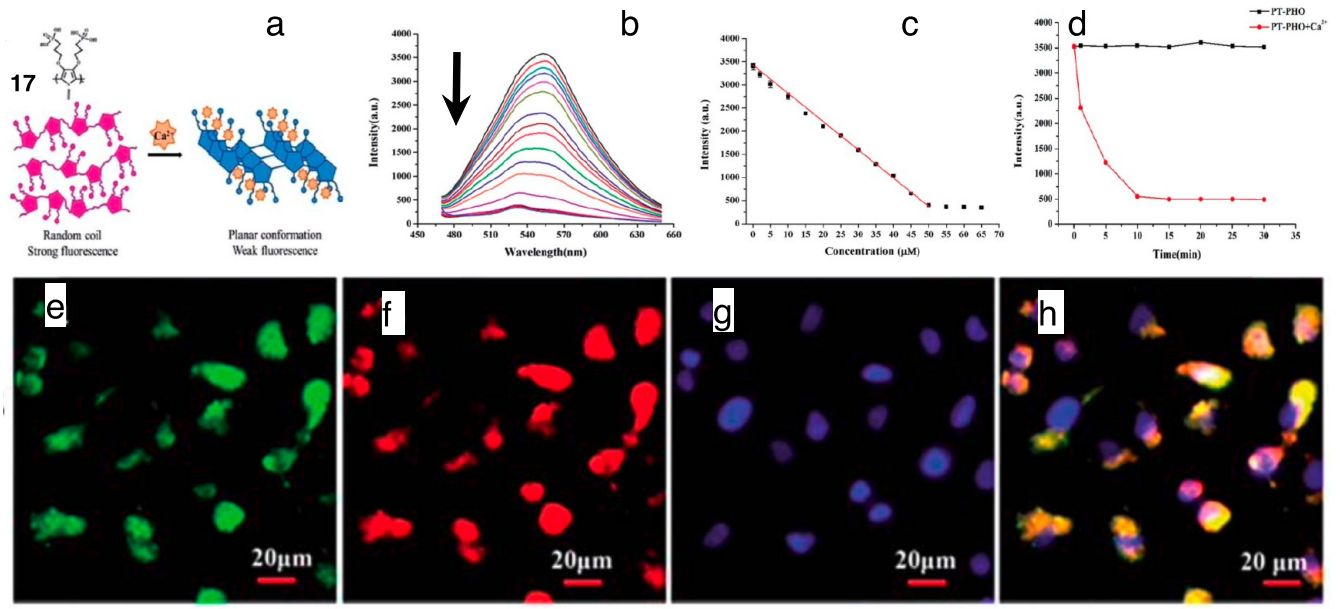

Figure 9. Detection of calcium ions in the lysosomal compartment. (a) The fluorescence sensing mechanism of PT-PHO (**17**) toward calcium ions. (b) Fluorescence quenching of **17** with the addition of calcium ions (0−65 mmol L^{-1}) at pH = 9 with excitation at 450 nm. (c) Change in the emission intensity measured at emission maxima with increasing concentration of calcium ions. (d) Kinetic monitoring of the fluorescence intensity of 50 mmol L^{-1} **17** upon addition of 50 mmol L^{-1} calcium ions. Colocalization imaging of **17**, Lyso-Tracker Red, and DAPI. (e) Fluorescence image of **17**. (f) Fluorescence image of Lyso-Tracker Red. (g) Fluorescence image of DAPI. (h) A merged image of (e−g). Scale bar: 20 μm. Reprinted with permission from ref 24. Copyright 2019, Royal Society of Chemistry.

endogenous Zn^{2+} ions was confirmed by treating cervical cancer cells with the zinc chelator *N,N,N,N*-tetrakis(2-pyridylmethyl)-ethylenediamine (TPEN) under oxidative stress conditions (Figure 7b).

Furthermore, the team of Xu demonstrated highly selective sensing of Zn^{2+} using the fluorescent naphthalimide derivative DR (**15**) as given in Figure 7c.[21] The probe was elegantly designed with *N,N*-bis(2-pyridylmethyl)ethylenediamine (BPEN) as a ligand and morpholine as a lysosome directing group. The synthesized probe showed weak fluorescence at pH 7.4 primarily attributed to the photoinduced transfer of electrons from the morpholine nitrogen and aniline nitrogen to the naphthalimide core. However, the binding of Zn^{2+} revealed a remarkable increment in the fluorescence intensity at 550 nm upon excitation at 450 nm (Figure 7d). The limit of detection (LOD) and binding constant were determined to be 15 nmol/L and 4.9×10^8 L/mol, respectively. The confocal laser scanning microscopic (CLSM) images revealed the ability of the probe to accumulate in the lysosomes of the MCF-7 cells. Additionally, the authors demonstrated that when SH-SY5Y cells were subjected to H_2O_2 stimulation, the occurrence of the endogenous Zn^{2+} release was evident. This was confirmed by monitoring the changes in fluorescence following cell treatment with H_2O_2 and the membrane-permeable zinc chelator TPEN.

2.4. Detection of Potassium ion (K^+). Xu and co-workers have employed DNA triangular prisms (DTPs) as the carrier for the detection of potassium ions in the lysosomal compartment.[22] The researchers have introduced a potassium-selective aptamer (KH) (Figure 8a) conjugated with three edges in the middle. For the simultaneous and fluorometric detection of potassium ions in lysosomes a fluorophore/Black Hole Quencher (BHQ) pair was used. For the detection of potassium ions Cy3/BHQ2 and for the detection of pH Cy5/BHQ2 dye pairs were selected (Figure 8b). The potassium-aptamer contains four groups of GGG and is expected to form a stable G-quadruplex in the presence of potassium. The DTP KH (**16**) probe has advantages over other existing probes as it detects multisignal simultaneous detection that can ensure the spatiotemporal consistency of detection results, which is suitable for studying the target with correlation. The conformational changes of **16** result in fluorescence resonance energy transfer. This was evident from the remarkable fluorescence intensity quenching of Cy3, which was utilized to monitor the concentration of potassium ions. The results demonstrated good potassium ion selectivity and a dynamic detection range of 5−200 mM. The results showed that **16** almost completely reacted with potassium ions after incubation at 37 °C for 30 min. The authors have utilized the gradual relative change in the fluorescence intensity against the concentration of potassium ions to quantify the signal response. The developed system is very selective toward potassium ions compared to other physiologically relevant cations.

2.5. Detection of Calcium (Ca^{2+}). Calcium efflux from the lysosomal compartment is thought to be important for signal transduction, organelle homeostasis, and organelle communications. Ca^{2+} concentration is ca. 5000-fold higher in the lysosomal lumen (∼0.5 mM) compared to the cytosol (∼100 nM).[23] Therefore, development of a novel Ca^{2+} ion sensor remains in the forefront of current research. In 2019, Feng and co-workers have designed and synthesized the new water-soluble polythiophene derivative poly[((thiophene-3,4-diylbis-(oxy))bis(propane-3,1-diyl))bis(phosphonic acid)] (PT-PHO, **17**), which displays a "turn off" fluorescent response for calcium ions detection.[24] Under optimal conditions, PT-PHO exhibits high selectivity and sensitivity toward calcium ions among selected biological metal ions. The fluorescence intensity of PT-PHO shows a linear response toward calcium ions in the range of 0.05−50 mmol L^{-1} with a limit of detection (LOD) value of 44

https://doi.org/10.1021/acsomega.3c08606
ACS Omega 2024, 9, 13494−13508

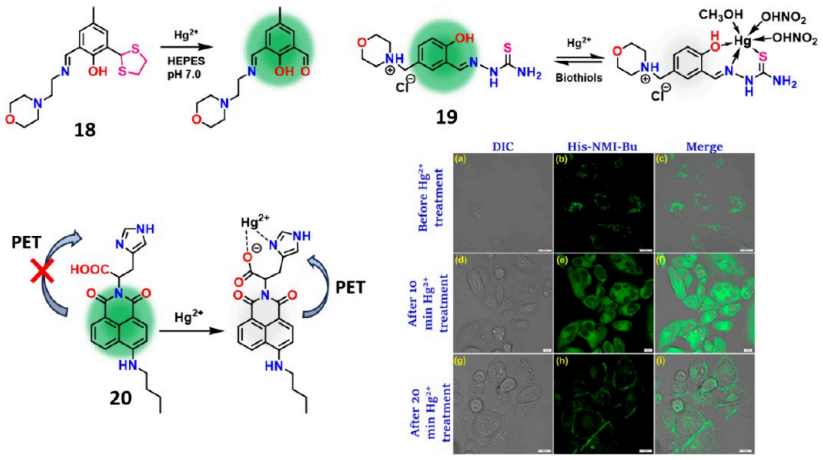

Figure 10. Schematic representation of the mechanism of action in molecules **18**−**20** for sensing Hg^{2+} ion and live cell images for lysosomal Hg^{2+} detection in BHK-21 cells using **20** depicting lysosomal membrane fusion with plasma membrane through lysosomal exocytosis.

nmol L^{-1}. When calcium ions were added, the conformation of PT-PHO changes from a randomly coiled morphology to a planar π-stacking aggregation morphology, resulting in significant emission quenching. In addition, PT-PHO selectively localizes in the lysosomal compartment. The fluorescence intensity of PT-PHO in the lysosomal compartment decreases with the increase of calcium ion concentration (Figure 9). Thus, it could be used for imaging and detecting calcium ions in lysosomal compartments in the cells.

2.6. Detection of Hg^{2+}. Mercury stands out in the extensive family of heavy metals for its notoriety as one of the most harmful and toxic heavy elements, capable of causing detrimental effects on living organisms. Mercury has the ability to trigger inflammatory and autoimmune responses in both human and experimental animal models. This is often attributed to its tendency to accumulate in lysosomal compartments and boost cathepsin B activity, which plays a significant role in engaging innate immune processes in mercury-induced inflammation and autoimmunity.[25] In the context of emphasizing the significance of mercury within lysosomes, we will delve into the latest advancements in detecting and monitoring lysosomal mercury levels.

Chattopadhyay and co-workers have designed and synthesized a 4-methyl-2,6-diformylphenol-derived fluorophore (Lyso-HGP, **18**) for lysosomal detection of Hg^{2+}.[26] **Probe 18** shows "turn-on" selective fluorescent detection of Hg^{2+} ions in a HEPES buffer solution (10 mM, DMSO 1%) of pH 7.0 at 37 °C through the transformation of 1,3-dithiolane into the highly fluorescent formyl-functionalized derivative Lyso-HGP-CHO (Figure 10). The turn-on response was observed at 530 nm when excited at 440 nm. This synthesized compound is capable of detecting a trace level of Hg^{2+} as low as 6.82 nM. The presence of a morpholine moiety directed the probe to the lysosomal compartment of the cells. They further applied the probe to detect Hg^{2+} in an MCF7 live cell sample. Moreover, the authors assessed the utility of the probe to detect this toxic heavy metal in biological samples and environmental samples.

In 2021, Xu and co-workers developed a water-soluble thiosemicarbazone compound (**19**) based on salicylaldehyde for the purpose of detecting Hg^{2+} ions (Figure 10).[27] The probe exhibited emission maxima at 480 nm when excited at 330 nm in HEPES buffer (50 mM, pH = 5.0). This emission intensity decreases in response to the presence of Hg^{2+}. The binding interaction between the probe and Hg^{2+} ions followed a 1:1 binding model with a binding constant of 5.00×10^4 M^{-1}, and the limit of detection for Hg^{2+} was found to be 0.52 μM. The probe exhibited reversibility when the probe-Hg^{2+} complex was exposed to biothiols (Cys, Hcy, and GSH). The lysosomal localization of the probe was confirmed through the utilization of commercially available LysoTracker Red, with a Pearson correlation coefficient value of 0.79. The authors investigated the applicability of the probe to detect Hg^{2+} in live cells. They observed a decrease in blue emission from HeLa cells upon introducing Hg^{2+}, which was then restored after the addition of biothiols.

Our group introduced histidine to the 1,8-naphthaimide **20** for sensing mercury and attaching butyl amine to the 4-position for an efficient intramolecular charge transfer process.[28] The absorption maxima was 455 nm in water and emission at 560 nm with a large Stokes shift value of 105 nm. The fluorescence intensity decreased with the addition of Hg^{2+} to the probe. The chelation induced fluorescence quenching due to static quenching, causing PET from naphthalimide to Hg^{2+}-ligand. The probe and Hg^{2+} in the 1:1 binding model was investigated through a Job's plot, and the binding constant was evaluated to be $(6.9 \pm 0.1) \times 10^6$ M^{-1}. The limit of detection (LOD) value in the MES buffer was calculated as 0.52 μM. The system can be utilized as a paper-based sensor for the detection of Hg^{2+}. Further, the applicability of the probe to detect intracellular Hg^{2+} was assessed in BHK-21 cells. Interestingly, the probe was localized in the lysosomal compartment of the cells, and we observed that lysosomal exocytosis occurred on introducing mercury to the cells causing the fusion of the lysosomal membrane with the plasma membrane (Figure 10).

2.7. Detection of Pd^0 and Pd^{2+}. Palladium finds extensive applications in electronics, dental restorations, and the automotive sector.[29] Consequently, a substantial quantity of palladium is introduced into both living and nonliving systems, potentially leading to various health risks. Researchers investigated that the hydrolytic enzymes located within lysosomal compartments undergo deactivation when they interact with Pd^{2+}, which binds to thiol groups or other negatively charged constituents of the enzyme.[30] The utilization of suitably customized fluorescent probes assists in detecting, monitoring, and comprehending the harmful impact of the Pd^{2+} ion on living systems.

In this direction, Zhong and team developed a fluorescent derivative of phthalimide PPA (**21**) bearing an excited-state

https://doi.org/10.1021/acsomega.3c08606
ACS Omega 2024, 9, 13494−13508

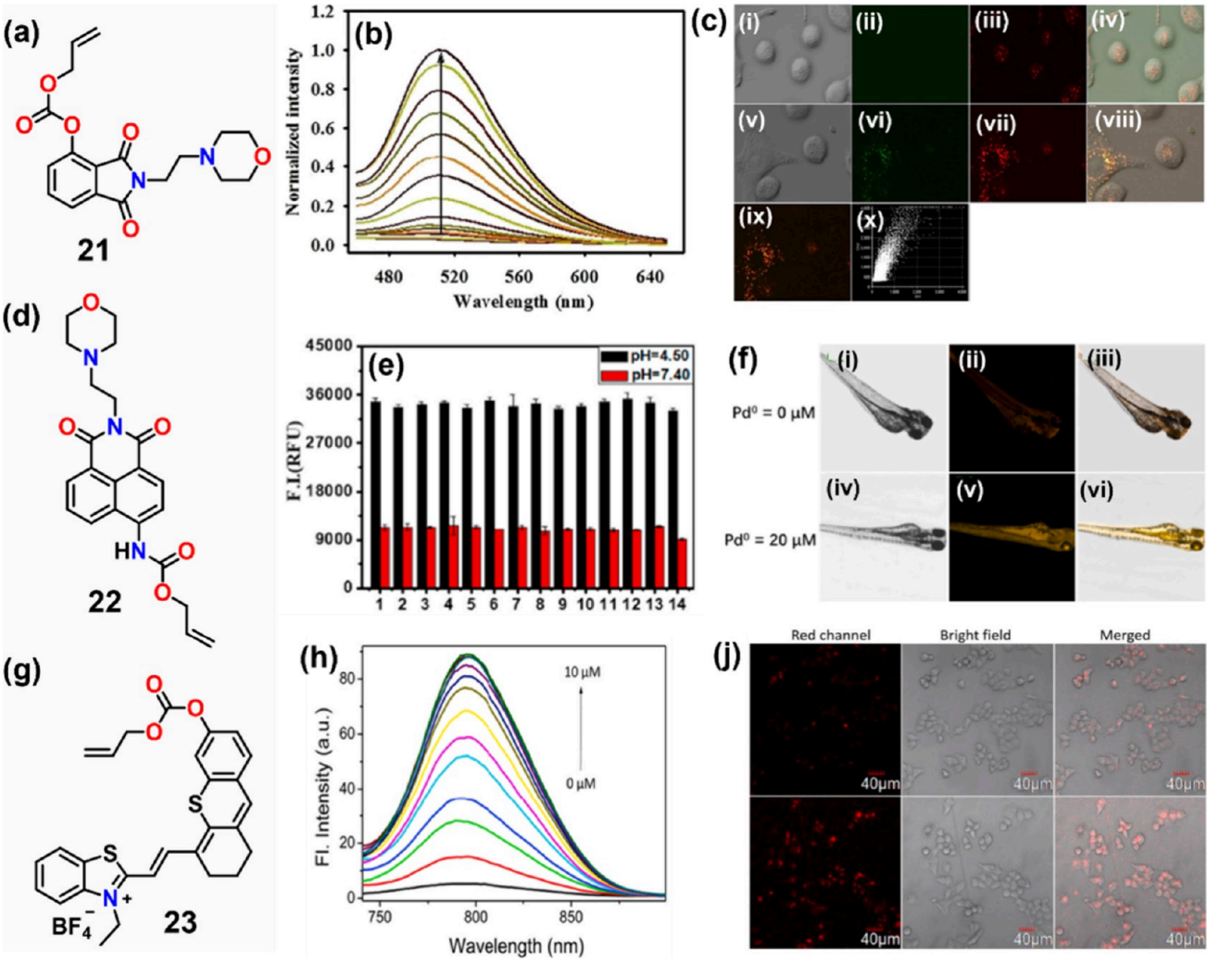

Figure 11. (a, d, g) Chemical structures of probes **21**−**23**, respectively, (b) Emission spectra of probe **21** (10 μM) with different concentrations of $Pd(PPh_3)_4$ (0−18 equiv) in CH_3CN-PBS solution (2:8, v/v, 50 mM, pH 7.4), (c) Fluorescence images of A549 cells treated with probe **21** (10 μM) and LysoTracker Red DND-99 (1 μM) for 30 min: (i) bright-field image; (ii) green channel; (iii) red channel; (iv) overlay of (i)−(iii); with $Pd(PPh_3)_4$ (v) brightfield image; (vi) green channel; (vii) red channel, (viii) overlay image of (v) and (vi); (ix) overlay image of (vi) and (vii); (x) correlation plot of LysoTracker Red DND-99 and **21** intensities. (c) is reprinted with permission from ref 29. Copyright 2018, Elsevier. (e) Selectivity assay for probe **22** with different metal ions Cu^+, Cd^{2+}, Co^{2+}, Cu^{2+}, Mn^{2+}, Sr^{2+}, Ba^{2+}, Fe^{2+}, Ni^{2+}, Zn^{2+}, Ca^{2+}, Al^{3+}, PBS, and Pd^0. (f) Zebrafish treated with probe **22** (10 μM) followed by treatment with PBS buffer (i−iii) and 20 μM Pd^0 for 75 min at 37 °C, λ_{ex} = 488 nm (iv−vi) (e, f) is reprinted with permission from ref 31. Copyright 2021, Elsevier. (g) Chemical structure of compound **23**. (h) Fluorescence response of probe **23** toward Pd^{2+} (0−10) μM. (j) Fluorescence images of HeLa cells incubated with only probe **23** for 30 min (upper panel) and probe and $PdCl_2$ (1 μM) (lower panel λ_{ex} = 635 nm, λ_{em} = 700−800 nm). (h−j) is reprinted with permission from ref 30. Copyright 2021, Elsevier.

intramolecular proton transfer (ESIPT) property for detecting Pd^{2+} (Figure 11a).[29] The probe conjugated with a palladium-responsive allyl carbamate moiety exhibited weak fluorescence due to ESIPT in CH_3CN-PBS solution (2:8, v/v, 50 mM, pH 7.4). However, the subsequent addition of Pd^{2+} (0−18 equiv) restored the emission at 511 nm via a palladium-catalyzed deallylation reaction (Figure 11b). Furthermore, the probe exhibited promising effectiveness in selectively and sensitively detecting palladium within the lysosomes of the lung cancer A549 cells (Figure 11c).

Subsequently, the lysosome-targeting dual-analyte fluorescent probe DPPP (**22**) was designed and synthesized by Wang for the recognition of pH and palladium by using two different emission channels (Figure 11d).[31] The probe consisted of a morpholine moiety accountable for enhanced response toward pH at 485 nm. Also demonstrated an intramolecular charge transfer (ICT) mediated "turn-on" fluorescence response at 545 nm owing to the detection of Pd(0) via an allyl carbamate group. Selectivity studies revealed the fluorogenic response of the probe only toward Pd(0) even in the presence of common Pd (Pd^{2+}/Pd^{4+}) variants and biologically relevant analytes (Figure 11e). The LOD was found to be 9 nM. The authors successfully demonstrated the variation in pH level and Pd(0) concentrations in lysosomes of HeLa cells and zebrafish models (Figure 11f). However, the aforementioned probes have shorter excitation and emission wavelengths, which limit their extensive utilization for *in vivo* models.

Subsequently, the benzothiazole-thioxanthene dye BTX-A (**23**) with emission in the near-infrared (NIR) region has been successfully utilized by Wang and co-workers for Pd^{2+} sensing (Figure 11g).[30] The authors utilized a "protection−deprotection" strategy with the allyl carbonate as the specific Pd^{2+}-responsive group. The interaction of the probe with Pd^{2+} furnished a red shift in the absorption maximum from 585 to

https://doi.org/10.1021/acsomega.3c08606
ACS Omega 2024, 9, 13494−13508

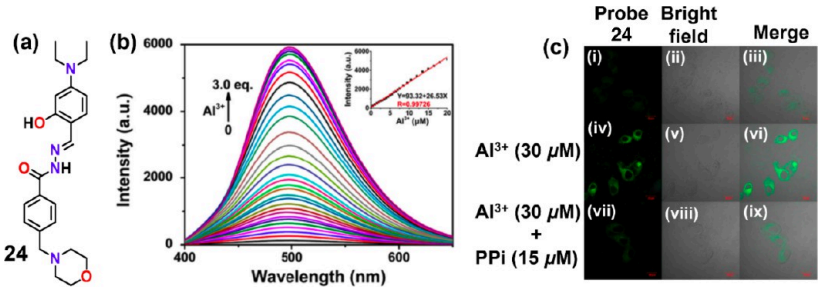

Figure 12. (a) Chemical structure of probe **24**. (b) Changes in emission intensity of probe **24** with progressive addition of Al^{3+} (0−3.0 equiv). (c) Fluorescence microscopic images showing the HeLa cells treated with **24** (10 μM) in the absence and presence of Al^{3+} and PPi ions. Reprinted with permission from ref 33. Copyright 2022, Elsevier.

750 nm accompanied by a visual color change to cyan from blue. Meanwhile, enhancement in emission intensity was observed at 795 nm upon the addition of Pd^{2+} in PBS buffer solution (10 mM, pH 7.4, containing 25% EtOH as a cosolvent) as shown in Figure 11h. The real sample analysis was performed by detecting the Pd^{2+} in tap water and pharmaceutical products. Promising spectroscopic investigations encouraged the authors to enquire into live cell imaging studies with BTX-A. The biocompatible probe exhibited subcellular compartmentalization at lysosomes of HeLa cells with efficient sensing of Pd^{2+} (Figure 11j).

2.8. Detection of Aluminum (Al^{3+}). Aluminum, being the third most abundant metal ion on the earth's crust, is considerably used in aerospace, food, pharmaceutical, and transportation industries. The success of aluminum in diverse fields of modern materials can be ascribed to its high thermal and electrical conductivity with great resistance to corrosion and easy deformation. Aluminum is intrudes into the biosphere through air, diet, and medication. The accumulation of unwanted aluminum retards the functions of the central nervous system (CNS), resulting in neurodegenerative disorders such as Alzheimer's and Parkinson's.[32] Surprisingly, the aluminum adjuvants used in vaccinations cause a massive burden to mankind. At the suborganelle level, aluminum deposits at the lysosomal compartments of the cell. Researchers have found that the soluble form of aluminum will be extracted from the uterus and ovary cells through the lysosomes of the cells. Therefore, the consequence of burgeoning exposure and accumulation caused by the noxiousness of aluminum in the biotic system must be seriously accounted for. Thus, the fluorescent probes tailored with an Al^{3+} coordinating site and lysosome targeting moiety are the best choice for selective and sensitive detection of Al^{3+}.

Xu and co-workers developed the hydrazone-based fluorescent probe **24** for Al^{3+} and pyrophosphate (PPi) detection (Figure 12a).[33] The probe showed a weak emission at 510 nm with a quantum yield of 0.079. However, the emission intensity at 510 nm increased enormously with an increase in the concentration of Al^{3+} ions (QY = 0.28) in HEPES buffered solution (20 mM, pH = 5.0) as shown in Figure 12b. The reversibility of the process was achieved by the addition of PPi, which completely quenched the emission of the probe-Al^{3+} complex. The live cell imaging studies revealed the complete accumulation of the probes in the lysosomes of the cell with a Pearson's correlation coefficient (PCC) of 0.88. Moreover, the efficiency of the probe for bioimaging of Al^{3+} and PPi was performed in the HeLa cells. The cells treated with the probe showed green fluorescence upon Al^{3+} (30 μM) addition and the fluorescence faded after PPi (15 μM) addition (Figure 12c).

2.9. Detection of Trivalent Metal Ions. In this section we will discuss the recent research articles on fluorescent sensors for detection of different trivalent metal ions like Fe^{3+}, Al^{3+}, In^{3+}, Ga^{3+}, and Cr^{3+}. In 2019, the Fu team employed a naphthalene derivative known as N-*p*-chlorophenyl-4-(2-aminoethyl)-morpholine-1,8-naphthalimide (CMN, **25**) as an effective chemosensor for the detection of trivalent metal ions, including Fe^{3+}, Al^{3+}, and Cr^{3+} (Figure 13a).[34] Upon gradually introducing

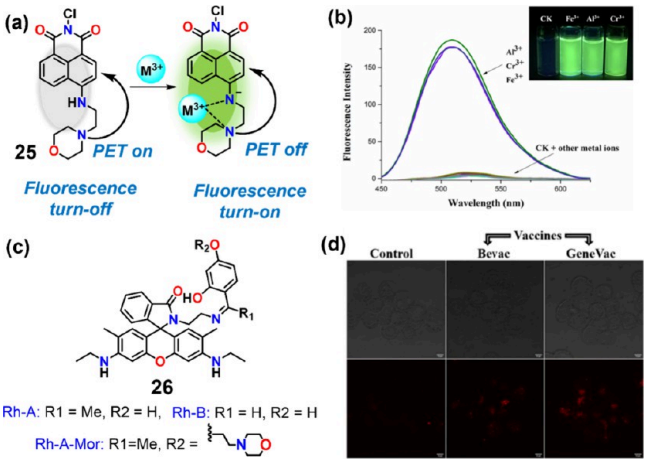

Figure 13. (a) Chemical structure and proposed mechanism for M^{3+} ions using probe **25**, (b) Variation in emission response of probe **25** in the presence of various metal cations (K^+, Na^+, Ag^+, Mg^{2+}, Zn^{2+}, Cu^{2+}, Ni^{2+}, Ba^{2+}, Ca^{2+}, Hg^{2+}, Pb^{2+}, Mn^{2+}, Co^{2+}, Cr^{3+}, Al^{3+}, Fe^{3+}, Au^{3+}, Fe^{2+}, Cr^{6+}, and In^{3+}) in methanol. Inset: images of vials with and without trivalent metal ions), (b) is reprinted with permission from ref 34. Copyright 2019, Elsevier. (c) Chemical structure of chemosensors **26**. (d) Confocal microscopic images of HeLa cells incubated with Rh-A-Mor (1 μM) followed by treatment with aluminum adjuvants (Bevac and Genevac, each with an aluminum concentration of 200 μM; control images are in the absence of treatment with adjuvants). (d) is reprinted with permission from ref 32. Copyright 2023, Royal Society of Chemistry.

trivalent metal ions, the probe CMN exhibited a "turn-on" fluorescence response, marked by visible color changes from CMN with visible color changes from pale yellow to deep yellow. The probe specifically recognized trivalent metal ions with a limits of detection of 0.65, 0.69, and 0.68 μM for Fe^{3+}, Al^{3+}, and Cr^{3+} ions, respectively (Figure 13b). Mechanistically, the weak emission of the probe was a result of PET from morpholine nitrogen to the naphthalimide core. However, upon the addition of trivalent metal ions, the morpholine nitrogen participated in complex formation inhibiting the process of PET, resulting in a turn-on response. The probe-bearing morpholine-naphthalimide platform illustrated exceptional capability for

https://doi.org/10.1021/acsomega.3c08606
ACS Omega 2024, 9, 13494−13508

Table 1. Reported Lysosomal Targeting Probes for Metal Cation Detection

				wavelength/nm				
sensor	detection method	LOD	solvent	λ_{ex}	λ_{em}	$K/10^4$ M	live cell imaging and *in vivo* imaging	ref
1	fluorometric	50 nM	HEPES buffer-dioxane (7:3 v/v)	630	665		HepG2 cells and SH-SY5Y cells	8
2	fluorometric		HEPES buffer-dioxane (7:3 v/v)				SH-SY5Y cells	8
3	colorimetric and fluorometric	0.037 μM	Tris-HCl buffer solution	471	531		HeLa cells and zebrafish	9
4	fluorometric	0.64 μM	water	365	450		HeLa cells	10
5	fluorometric	0.05 μM	acetonitrile/Tris-HCl buffer (10 mM, pH 7.3, v/v 3:1)	510	580	1.54×10^3	SH-SY5Y and ws1 cells	11
6	fluorometric	65.2 nM	HEPES buffer (pH 7.4; EtOH: H_2O = 5%; v/v)	405	510		HeLa cells	12
7	fluorometric	0.44 μM	water	452	560	6.9 ± 0.7	HeLa cells	13
8	fluorometric	**8a** = 2.62×10^{-9} M **8b** = 4.51×10^{-9} M **8c** = 1.17×10^{-8} M	Tris-HCl (1 mM, pH 7.2)		541 (**8a**) 546 (**8b**) 540 (**8c**) 536 (**8d**)		HeLa cells	15
9	fluorometric	320 nM	CH_3CN-HEPES (4:1, v/v, pH = 7.4)	440		2.8	293T cells	14
10	fluorometric	19.40 nM	AcOH−NaOAc buffer (10 mM, pH 5.0)	360	440		HepG2 cells	16
11	fluorometric	6.79 nM	Tris-HCl buffer solution (2 mM, pH 7.4)	400	550	14.2	HeLa cells	17
12	fluorometric		methanol	610	660		SH-SY5Y cells	18
13	fluorometric	0.062 μmol L^{-1}	PBS buffer (EtOH:H_2O) = 1:99, pH = 7.4)	380	586		HeLa cells	19
14	fluorometric	369 nM (pH = 6)	PBS buffer (pH = 7.4)	390	530 (pH = 5) 610 (pH = 4, 5)		HeLa cells	20
15	fluorometric	15 nmol/L	0.1 mol/L TrisHCl buffer (0.5% DMSO, pH 5.0)	450	550	4.9×10^4	SH-SY5Y	21
16	fluorometric		TE buffer (10 mM Tris-HCl, 0.1 mM EDTA, pH = 8.0)				MCF-7 cells	22
17	fluorometric	44 nmol L^{-1}	NH_3−NH_4Cl buffer	450			A549 cells	24
18	fluorometric	6.82 nM	HEPES buffer (1% DMSO, 10 mM, pH 7.0)	440	530		MCF7 cells	26
19	fluorometric	0.52 μM	HEPES buffer (50 mM, pH = 5.0)	330	480	5.0	HeLa cells	27
20	fluorometric	0.52 μM	MES buffer	455	560	$6.9 \pm 0.1 \times 10^2$	BHK-21 cells	28
21	fluorometric	2.8×10^{-8} M	CH_3CN-PBS solution (2:8, v/v, 50 mM, pH 7.4)	400	511		A549 cells	29
22	fluorometric	9 nM	PBS buffer (10% DMSO; 10 mM)	445	545		HeLa cells and zebrafish	31
23	colorimetric and fluorometric	21.3 nM	PBS buffer (10 mM, pH 7.4, 25% EtOH)	680	795		HeLa cells	30
24	fluorometric	35.7 nM	HEPES buffer (20 mM, pH = 5.0, 1% DMSO)	370	510	2.6×10^2	HeLa cells	33
25	fluorometric	Fe^{3+} = 0.65 μM Al^{3+} = 0.69 μM Cr^{3+} = 0.68 μM	methanol	438	509	Fe^{3+} = 5.3 Al^{3+} = 3.3 Cr^{3+} = 4.9	methanol	34
26	colorimetric and fluorometric	Rh-A-mor = 0.10 μM Rh-A = 0.13 μM Rh-B = 0.17 μM	NaCl solution (ionic strength 20 mM, pH 6.0)	510	554	Rh-A-mor = 4.1 ± 0.27 Rh-A = 1.7 ± 0.13 Rh-B = 1.1 ± 0.05	HeLa cells	32

imaging trivalent metal cations (Fe^{3+}, Al^{3+}, and Cr^{3+}) in lysosomes of mouse myoblast (C2C12) cells.

In addition to this, recently, Koner and co-workers synthesized a series of rhodamine-benzaldehyde/acetophenone-based hybrid moieties as aqueous soluble trivalent metal ion sensors Rh-A, Rh-B, and Rh-A-Mor (**26**) as shown in Figure 13c.[32] In solution, all three probes selectively detected trivalent metal ions such as Al^{3+}, In^{3+}, Ga^{3+}, and Fe^{3+} through a "turn-on" colorimetric and fluorometric response. Considering the higher intake of aluminum by living organisms through dietary and medicinal sources, the authors considered Al^{3+} as a model trivalent metal ion to perform comprehensive spectroscopic and microscopic studies. Mechanistically, the complexation with Al^{3+} rendered the emergence of a new emission band at approximately 550 nm in NaCl solution (ionic strength 20 mM, pH 6.0) at 37 °C. According to the authors' observation, the ring opening and restoration of conjugation on the xanthene core is the sole effect of Al^{3+} coordination with rhodamine 6G derivatives. Similar to previous work, the reversibility of the phenomenon was achieved by fluorescence titration with PPi

https://doi.org/10.1021/acsomega.3c08606
ACS Omega 2024, 9, 13494−13508

Table 2. Concentration of Different Metal Cations in Lysosomes

metal ion	concentration/mM			ref
	lysosome	cytosol	extracellular fluid	
Na^+	~80−120	~12	~135−147	35,36
K^+	~2−50	~100−150	~3.5−5.0	36, 37
Mg^{2+}	~0.5 (~10)[a]	~4−5	~0.5−1.0	3, 36
Ca^{2+}	~0.5	~0.1 × 10^{-3}	~2.0	36, 38
Zn^{2+}	[b]	~0.1 × 10^{-6}	~0.01−0.02	36, 39, 40
Fe^{2+}/Fe^{3+}	~0.6[c]	~0.5−3.0[c]	~0.015−0.02 (Fe^{2+})	36, 41
Cu^+/Cu^{2+}	~1−5 × 10^{-3}	~10^{-6}	~0.01−0.02 (Cu^{2+})	36
Pd^{2+}, Hg^{2+} and other M^{3+}	not reported (These metal ions are intruded from the external environment)			

[a]Bound Mg^{2+} ions. [b]μM−mM. [c]In neuronal cells.

ions. Furthermore, the lysosome localizing probes successfully demonstrated the bioimaging and quantification of aluminum released by the aluminum adjuvants within the lysosomes of the HeLa cells (Figure 13d). Table 1 summarizes recent progress over the past five years.

3. CHALLENGES AND FUTURE OUTLOOK

The concentration of metal ions within cellular organelles, including lysosomes and cytosol, is linked to intracellular biochemical reactions and processes. Changes in these concentrations can impact various neurological conditions and cancers. Moreover, maintaining appropriate ion levels in the extracellular fluid is crucial for preserving cellular physiology (Table 2).[3,35−41]

Ion channels and transporter present in the lysosomal compartment play an essential role in regulating lysosomal homeostasis. There is a constant efflux of cations to maintain ionic homeostasis and the acidic environment in the lysosomal compartment. The function of most lysosomal hydrolases need an acidic environment with 100−1000-fold higher concentration of H^+ ions. An increase in the permeability of ions may alter the concentration gradient of metal ions across the lysosomal membrane and ultimately affect the various fusion events associated with endosomal trafficking. There are multiple methods such as using ionic fluxes, single-channel recording with purified protein reconstituted in lipid bilayers, and whole-lysosomal recording from artificially enlarged lysosomes are known for estimating the lysosomal ionic conductance. However, small-molecule-based fluorescence sensing methods suitable for selective sensing of metal ions are popular. Such methods allow us to visualize the dynamic changes in metal ion concentration inside the lysosomal compartment of live cells. However, the success in achieving selective detection of desired metal cations is limited to the *in vitro* level. *In vivo* detection requires:

- near-infrared emission (NIR) and two-photon absorption to achieve deep tissue penetration and animal imaging
- substantial Stokes shift to avoid autofluorescence
- aqueous solubility to prevent the lethal response to living system caused by using organic solvents
- photostability to prevent photobleaching of fluorophores upon continuous irradiation
- negligible cytotoxicity on living systems

In addition, current studies often fall short in providing quantitative assessments of concentration and dynamic changes during various physiological processes. To address this gap, there is a need for the development of lysosome-specific small fluorescent molecules with substantial excited-state lifetimes. This development could prove highly valuable, enabling the utilization of fluorescence lifetime imaging microscopy (FLIM) to visualize metal ion concentration and dynamic changes. Crucially, the modification in the lifetime of the probe should be linked to the concentration of particular metal ions within the lysosomal compartment, allowing for precise quantification of metal ion concentrations. The aforementioned properties will enhance the clinical utility of the developed fluorescent sensors for *in vivo* imaging purposes.

■ ASSOCIATED CONTENT

Supporting Information

The Supporting Information is available free of charge at https://pubs.acs.org/doi/10.1021/acsomega.3c08606.

Further information related to intracellular upregulation or downregulation of essential metal ions/ion channels and their role in cancer (PDF)

■ AUTHOR INFORMATION

Corresponding Author

Apurba Lal Koner − *Bionanotechnology Lab, Department of Chemistry, Indian Institute of Science Education and Research Bhopal, Bhopal 462066 Madhya Pradesh, India;* orcid.org/0000-0002-8891-416X; Email: akoner@iiserb.ac.in

Authors

Akshay Silswal − *Bionanotechnology Lab, Department of Chemistry, Indian Institute of Science Education and Research Bhopal, Bhopal 462066 Madhya Pradesh, India*

Kavyashree P. − *Bionanotechnology Lab, Department of Chemistry, Indian Institute of Science Education and Research Bhopal, Bhopal 462066 Madhya Pradesh, India*

Complete contact information is available at: https://pubs.acs.org/10.1021/acsomega.3c08606

Author Contributions

†A.S. and K.P. contributed equally to this work.

Notes

The authors declare no competing financial interest.

https://doi.org/10.1021/acsomega.3c08606
ACS Omega 2024, 9, 13494−13508

Biographies

Dr. Akshay Silswal obtained his doctoral degree in Chemistry from IISER Bhopal. During his doctoral research, he was involved in developing the fluorophore for targeting specific cellular organelles to understand their biophysics and sensing application. His current research is centered on advancing fluorophores and utilizing them for sensing and photocatalysis applications.

Dr. Kavyashree P. completed her MSc degree in chemistry from Mangalore University in 2017. In the same year, she started her doctoral studies under the supervision of Dr. Apurba Lal Koner, IISER Bhopal. Her research interest is synthesis of styryl-based fluorescent molecules and exploring their applications for detection of different analytes associated with neurodegenerative diseases.

Dr. Apurba Lal Koner is an Associate Professor at Department of Chemistry in IISER Bhopal. He obtained his Ph.D. in Chemistry from Jacobs University, Bremen, Germany. After postdoctoral work at the University of Oxford, he joined IISER Bhopal in 2012. One of his current research interests lies in the design and synthesis of novel fluorescent reporters for sensing and live-cell fluorescence imaging for understanding subcellular properties.

■ ACKNOWLEDGMENTS

We wish to acknowledge the financial support from the host institute IISER Bhopal. A.S. and K.P. thank CSIR, INDIA and IISER Bhopal, respectively, for their doctoral fellowship.

■ REFERENCES

(1) Carter, K. P.; Young, A. M.; Palmer, A. E. Fluorescent Sensors for Measuring Metal Ions in Living Systems. *Chem. Rev.* **2014**, *114* (8), 4564−4601.
(2) Hare, D. J.; New, E. J.; de Jonge, M. D.; McColl, G. Imaging metals in biology: balancing sensitivity, selectivity and spatial resolution. *Chem. Soc. Rev.* **2015**, *44* (17), 5941−5958.
(3) Xu, H.; Ren, D. Lysosomal Physiology. *Annu. Rev. Physiol.* **2015**, *77* (1), 57−80.
(4) Krämer, J.; Kang, R.; Grimm, L. M.; De Cola, L.; Picchetti, P.; Biedermann, F. Molecular Probes, Chemosensors, and Nanosensors for Optical Detection of Biorelevant Molecules and Ions in Aqueous Media and Biofluids. *Chem. Rev.* **2022**, *122* (3), 3459−3636.
(5) Unniram Parambil, A. R.; P, K.; Silswal, A.; Koner, A. L. Water-soluble optical sensors: keys to detect aluminium in biological environment. *RSCAdv.* **2022**, *12* (22), 13950−13970.
(6) Biswas, S.; Sharma, V.; Kumar, P.; Koner, A. L. Selective sensing of lysosomal iron(III) via three-component fluorescence-based strategy in living cells. *Sens. Actuators B: Chem.* **2018**, *260*, 460−464.
(7) Rizzollo, F.; More, S.; Vangheluwe, P.; Agostinis, P. The lysosome as a master regulator of iron metabolism. *Trends Biochem. Sci.* **2021**, *46* (12), 960−975.
(8) Hirayama, T.; Inden, M.; Tsuboi, H.; Niwa, M.; Uchida, Y.; Naka, Y.; Hozumi, I.; Nagasawa, H. A Golgi-targeting fluorescent probe for labile Fe(ii) to reveal an abnormal cellular iron distribution induced by dysfunction of VPS35. *Chem. Sci.* **2019**, *10* (5), 1514−1521.
(9) Chang, D.; Zhao, Z. H.; Shi, L. H.; Liu, W. L.; Yang, Y. X. Lysosome-targeted carbon dots for colorimetric and fluorescent dual mode detection of iron ion, in vitro and in vivo imaging. *Talanta* **2021**, *232*, 122423.
(10) Wu, Y. Q.; Cao, L.; Zan, M. H.; Hou, Z.; Ge, M. F.; Dong, W. F.; Li, L. Iron and nitrogen-co-doped carbon quantum dots for the sensitive and selective detection of hematin and ferric ions and cell imaging. *Analyst* **2021**, *146* (15), 4954−4963.
(11) Alhawsah, B.; Yan, B.; Aydin, Z.; Niu, X. Y.; Guo, M. L. Highly Selective Fluorescent Probe With an Ideal pH Profile for the Rapid and Unambiguous Determination of Subcellular Labile Iron (III) Pools in Human Cells. *Anal. Lett.* **2022**, *55* (12), 1954−1970.
(12) Li, X. R.; Qin, W. W. A novel dual-capability naphthalimide-based fluorescent probe for Fe3+ ion detection and lysosomal tracking in living cells. *RSCAdv.* **2022**, *12* (37), 24252−24259.
(13) Silswal, A.; Weslie, P.; Koner, A. L. Bioimaging of labile lysosomal iron through naphthalimide-based fluorescent probe. *Talanta* **2023**, *254*, No. 124147.
(14) Fu, Y.; Pang, X. X.; Wang, Z. Q.; Chai, Q.; Ye, F. A highly sensitive and selective fluorescent probe for determination of Cu (II) and application in live cell imaging. *Spectrochim. Acta, Part A* **2019**, *208*, 198−205.
(15) Gao, Y. G.; Liu, F. L.; Patil, S.; Li, D. J.; Qadir, A.; Lin, X.; Tian, Y.; Li, Y.; Qian, A. R. 1,8-Naphthalimide-Based Multifunctional Compounds as Cu(2+) Probes, Lysosome Staining Agents, and Non-viral Vectors. *Front. Chem.* **2019**, *7*, 616.
(16) Xu, T.; Huang, J.; Fang, M.; Sui, M.; Zhu, Y.; Shentu, Y.; Li, C.; Zhu, W. A novel "turn-on" fluorescent probe based on naphthalimide for the tracking of lysosomal Cu2+ in living cells. *New J. Chem.* **2020**, *44* (48), 21167−21175.
(17) Liu, L.; Duan, H.; Wang, H.; Miao, J.; Wu, Z.; Li, C.; Lu, Y. Lysosome-Targeting Fluorescence Sensor for Sequential Detection and Imaging of Cu2+ and Homocysteine in Living Cells. *ACS Omega* **2022**, *7* (38), 34249−34257.

https://doi.org/10.1021/acsomega.3c08606
ACS Omega 2024, 9, 13494−13508

(18) Priessner, M.; Summers, P. A.; Lewis, B. W.; Sastre, M.; Ying, L.; Kuimova, M. K.; Vilar, R. Selective Detection of Cu(+) Ions in Live Cells via Fluorescence Lifetime Imaging Microscopy. *Angew. Chem., Int. Ed.* **2021**, *60* (43), 23148−23153.
(19) Cheng, Z.; Jin, X.; Liu, Y.; Zheng, L.; He, H. An ESIPT-Based Fluorescent Probe for Aqueous Cu(+) Detection through Strip, Nanofiber and Living Cells. *Molecules* **2023**, *28* (9), 3725.
(20) Sudheesh, K. V.; Joseph, M. M.; Philips, D. S.; Samanta, A.; Kumar Maiti, K.; Ajayaghosh, A. pH-Controlled Nanoparticles Formation and Tracking of Lysosomal Zinc Ions in Cancer Cells by Fluorescent Carbazole−Bipyridine Conjugates. *ChemistrySelect* **2018**, *3* (8), 2416−2422.
(21) Duan, H.; Ding, Y.; Huang, C.; Zhu, W.; Wang, R.; Xu, Y. A lysosomal targeting fluorescent probe and its zinc imaging in SH-SY5Y human neuroblastoma cells. *Chin. Chem. Lett.* **2019**, *30* (1), 55−57.
(22) Li, X. Q.; Liu, X. N.; Jia, Y. L.; Luo, X. L.; Chen, H. Y.; Xu, J. J. Dual Recognition DNA Triangular Prism Nanoprobe: Toward the Relationship between K and pH in Lysosomes. *Anal. Chem.* **2021**, *93* (44), 14892−14899.
(23) Lloyd-Evans, E.; Morgan, A. J.; He, X.; Smith, D. A.; Elliot-Smith, E.; Sillence, D. J.; Churchill, G. C.; Schuchman, E. H.; Galione, A.; Platt, F. M. Niemann-Pick disease type C1 is a sphingosine storage disease that causes deregulation of lysosomal calcium. *Nat. Med.* **2008**, *14* (11), 1247−1255.
(24) Yang, T.; Hu, Z. R.; Liu, J. L.; Zhang, Z. Q.; Feng, G. D. A novel phosphonic acid functional polythiophene fluorescent sensor for Ca and its live cell imaging. *Anal Methods* **2019**, *11* (39), 4991−4997.
(25) Pollard, K. M.; Cauvi, D. M.; Toomey, C. B.; Hultman, P.; Kono, D. H. Mercury-induced inflammation and autoimmunity. *Biochim. Biophys. Acta* **2019**, *1863* (12), No. 129299.
(26) Sarkar, A.; Chakraborty, S.; Lohar, S.; Ahmmed, E.; Saha, N. C.; Mandal, S. K.; Dhara, K.; Chattopadhyay, P. A Lysosome-Targetable Fluorescence Sensor for Ultrasensitive Detection of Hg2+ in Living Cells and Real Samples. *Chem. Res. Toxicol.* **2019**, *32* (6), 1144−1150.
(27) Li, X. H.; Han, X. F.; Wu, W. N.; Wang, Y.; Fan, Y. C.; Zhao, X. L.; Xu, Z. H. Simple thiosemicarbazone "switch" sensing of Hg and biothiols in pure aqueous solutions and application to imaging in lysosomes. *J. Mol. Struct.* **2022**, *1250*, 131811.
(28) Roy, R.; Dutta, T.; Nema, S.; Koner, A. L. Detection of Lysosomal Hg Using a pH-Independent Naphthalene Monoimide-Based Fluoroprobe. *Chemosensors* **2023**, *11* (3), 184.
(29) Shen, Y.; Zhang, X.; Wu, Y.; Zhang, Y.; Liu, X.; Chen, Y.; Li, H.; Zhong, Y. A lysosome targetable fluorescent probe for palladium species detection base on an ESIPT phthalimide derivative. *Spectrochim. Acta, Part A* **2018**, *205*, 66−71.
(30) Liu, Q.; Li, J.; Liu, C.; He, S.; Zhao, L.; Zeng, X.; Wang, T. Developing a NIR emitting benzothiazolium-thioxanthene dye and its application for the design of lysosomes-targeting palladium(II) probe. *Dyes and Pigm.* **2021**, *196*, No. 109796.
(31) Xie, Z.; Zhou, Y.; Fu, M.; Ni, L.; Tong, Y.; Yu, Y.; Li, N.; Yang, Z.; Zhu, Q.; Wang, J. A 1,8-naphthalimide-based lysosome-targeting dual-analyte fluorescent probe for the detection of pH and palladium in biological samples. *Talanta* **2021**, *231*, No. 122365.
(32) P, K.; Unniram Parambil, A. R.; Silswal, A.; Pramanik, A.; Koner, A. L. Trivalent metal ion sensor enabled bioimaging and quantification of vaccine-deposited Al(3+) in lysosomes. *Analyst* **2023**, *148* (11), 2425−2437.
(33) Song, Y. F.; Cai, H. X.; Wu, W. N.; Zong, H. T.; Li, M.; Wang, Y.; Fan, Y. C.; Xu, Z. H. A simple hydrazone probe for recognition of Al(3+) and PPi and its applicability in lysosomal imaging. *Spectrochim. Acta, Part A* **2022**, *268*, No. 120680.
(34) Ye, F.; Wu, N.; Li, P.; Liu, Y.-L.; Li, S.-J.; Fu, Y. A lysosome-targetable fluorescent probe for imaging trivalent cations Fe3+, Al3+ and Cr3+ in living cells. *Spectrochim. Acta, Part A* **2019**, *222*, 117242.
(35) Li, P.; Gu, M.; Xu, H. Lysosomal Ion Channels as Decoders of Cellular Signals. *Trends Biochemi. Sci.* **2019**, *44* (2), 110−124.
(36) Bischof, H.; Burgstaller, S.; Waldeck-Weiermair, M.; Rauter, T.; Schinagl, M.; Ramadani-Muja, J.; Graier, W. F.; Malli, R. Live-Cell Imaging of Physiologically Relevant Metal Ions Using Genetically Encoded FRET-Based Probes. *Cells* **2019**, *8* (5), 492.
(37) Burgstaller, S.; Bischof, H.; Matt, L.; Lukowski, R. Assessing K+ ions and K+ channel functions in cancer cell metabolism using fluorescent biosensors. *Free Radic. Biol. Med.* **2022**, *181*, 43−51.
(38) Barbonari, S.; D'Amore, A.; Palombi, F.; De Cesaris, P.; Parrington, J.; Riccioli, A.; Filippini, A. Relevance of lysosomal Ca2+ signalling machinery in cancer. *Cell Calcium* **2022**, *102*, No. 102539.
(39) Gu, M.; Hu, M.; Minckley, T.; Pinchi, P.; Xu, H.; Qin, Y.; Du, W. A protocol to measure lysosomal Zn2+ release through a genetically encoded Zn2+ indicator. *STAR Protocols* **2022**, *3* (2), No. 101453.
(40) Minckley, T. F.; Zhang, C.; Fudge, D. H.; Dischler, A. M.; LeJeune, K. D.; Xu, H.; Qin, Y. Sub-nanomolar sensitive GZnP3 reveals TRPML1-mediated neuronal Zn2+ signals. *Nat. Commun.* **2019**, *10* (1), 4806.
(41) Reinert, A.; Morawski, M.; Seeger, J.; Arendt, T.; Reinert, T. Iron concentrations in neurons and glial cells with estimates on ferritin concentrations. *BMC Neurosci.* **2019**, *20* (1), 25.

https://doi.org/10.1021/acsomega.3c08606
ACS Omega 2024, 9, 13494−13508